VOLUMINA JURASSICA, 2024, XXII: 25–34
DOI: 10.7306/VJ.22.3

From Jurassic deep-sea life to deterministic Solar System dynamics: Insights from recurrence plot analysis of ichnological data, Toarcian, Llanbedr (Mochras Farm) borehole, UK

Krzysztof NINARD[1], Alfred UCHMAN[1], Grzegorz PIEŃKOWSKI[2], Stephen P. HESSELBO[3]

Key words: recurrence plots, orbital cycles, ichnofossils, mathematical methods.

Abstract. Bioturbation structures preserved in the c. 260 m long Toarcian section of the Llanbedr (Mochras Farm) borehole (Wales, UK) display cyclic occurrences influenced by astronomical forcing. Depth-domain data series of ichnotaxa distribution were analysed using recurrence plots, which allow observation of cyclic patterns across various scales simultaneously and assessment of the varied responses of different tracemakers to the influence of particular orbital terms. *Phycosiphon* and *Schaubcylindrichnus* occurrences reflect the combined effect of precession, obliquity, and short eccentricity. In turn, conditions favouring the development of undulated bedding and the *Thalassinoides* and *Trichichnus* tracemakers were primarily controlled by the long eccentricity. Disruptions in the plots likely result from average sedimentation rate changes, and stress conditions experienced by benthic fauna during the latter stages of the Early Toarcian carbon isotope excursion. Generally, the plots reveal patterns characteristic of systems governed by deterministic chaos, with pronounced cyclic components.

INTRODUCTION

The Llanbedr (Mochras Farm) borehole (Wales, UK) – commonly referred to as Mochras – cored an extraordinarily thick and complete succession of Lower Jurassic mudstone deposits. This succession represents an infill of the extensional Cardigan Bay Basin, which during the Early Jurassic was located at a mid-palaeolatitude (c. 35–40°N) in the axial part of the Laurasian Seaway (Fig. 1, Woodland, 1971; Dobson, Whittington, 1987; Copestake, Johnson, 2013; Hesselbo *et al.*, 2013). The c. 260 m long (610–863.5 m below surface) Toarcian section of the core has been subject to numerous studies including sedimentology, integrated stratigraphy, and palaeoclimatology, most recently outlined and supplemented by Pieńkowski *et al.* (2024).

Based on visual inspection of the core, Pieńkowski *et al.* (2024) distinguished four orders of cycle duration from the Mochras Toarcian. A hierarchical ordering of cycles was adopted that refers to astronomically-paced climatic cyclicities, and thus differs from conventional ordering of geotectonic cycles that also include very long periods (>10 Ma). The distinction between cycles was based on the integrated set of ichnological features, taking into consideration all ichnotaxa present in the section. The 4th-order cyclicity is interpreted as either precession (c. 20 kyr), obliquity (c. 38 kyr, Waltham, 2015), or a superposition of both. Distinction

[1] Jagiellonian University, Faculty of Geography and Geology, Gronostajowa 3a, 30-387 Kraków, Poland; e-mail: krzysztof.ninard@uj.edu.pl; alfred.uchman@uj.edu.pl.

[2] Polish Geological Institute – National Research Institute, Rakowiecka 4, 00-975 Warszawa, Poland [Grzegorz Pieńkowski died in April 2023].

[3] Camborne School of Mines, Department of Earth and Environmental Sciences, University of Exeter, Penryn Campus, Cornwall TR10 9FE, UK; e-mail: s.p.hesselbo@exeter.ac.uk.

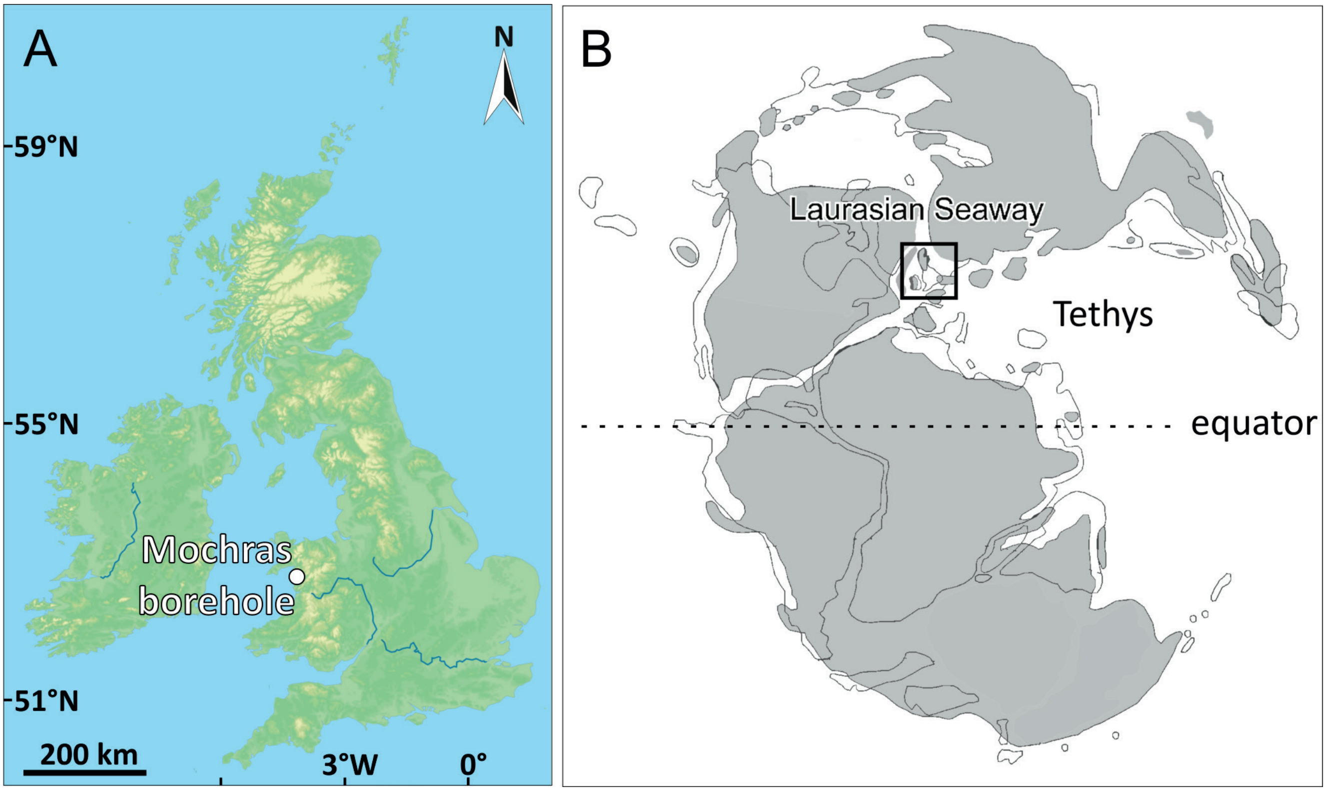

Fig. 1. Location maps

A. Location of the Mochras borehole in Great Britain; **B.** British Isles against the background of the Toarcian palaeogeography (the map based on Pieńkowski *et al.*, 2024)

between precession and obliquity cycles was unfeasible in direct observation in the face of a slow, and to some degree, fluctuating sedimentation rate. Short eccentricity (c. 100 kyr) and long eccentricity (c. 405 kyr; Kent *et al.*, 2018) are distinguished as 3rd and 2nd-order cycles, respectively. The 1st order is attributed to c. 2.4 Myr cycles, caused by eccentricity modulation resultant of Earth-Mars secular resonance (see *e.g.*, Hinnov, 2000). Independently of visual observation, Pieńkowski *et al.* (2024) detected the 4th and 3rd order cycles by applying numerical spectral analysis of binary time series representing occurrences of particular ichnotaxa. The average sedimentation rate for the whole Toarcian is estimated at 4.1 cm/kyr.

Recurrence plots can provide information about the characteristics of the underlying dynamics of the data, including spatio-temporal scales of periodicity. The recurrence plot technique originated in the field of nonlinear system physics (Marwan *et al.*, 2007). Along with the current trend of applying this method in the analysis of experimental data, it is rapidly gaining popularity among investigators of palaeoclimatological and geophysical data (Marwan *et al.*, 2021). Westerhold *et al.* (2020) demonstrated the utility of isotope data recurrence plots in their study of climate change patterns over the whole Cenozoic. In the field of palaeontology, the use of recurrence plots was introduced by Spiridonov (2017) based on conodont abundance data. Subsequent works by Spiridonov *et al.* (2019, 2020) demonstrated the usefulness of recurrence plots on other palaeontological datasets and elucidated approaches to their interpretation.

In the present study, the recurrence plot technique is for the first time employed for the analysis of ichnological data from the stratigraphic section, based on the Toarcian ichnotaxa occurrence time series from the Mochras borehole. The present contribution aims to explore this unique dataset, demonstrate how particular ichnotaxa data register orbital forcing, and compare their response to the cyclic astronomical signal.

MATERIAL AND METHODS

Regarding occurrences of trace fossils, two distinct morphotypes of *Phycosiphon incertum* (*Ph*2, and *Ph*3), *Thalassinoides*, *Schaubcylindrichnus*, *Trichichnus,* as well as intervals with undulated bedding, were used to compile discrete binary time series because of the general abundances, palaeoenvironmental significance, and ease of recognition. Ranges of trace fossils and undulated bedding (see Pieńkowski *et al.*, 2024, fig. 2) were binarized by automated digitalization using the proprietary Pascal-based BinartGeo program at one-pixel resolution. The program converts monochrome raster logs along a given line, outputting white pixels as zeros and black pixels as ones. Resultant time series consist of 11,289 binary digits for each category. Due to automated digitalization of graphical data, length of derivative binary time series increased four-fold compared to the manually digitized time series analysed in Pieńkowski *et al.*, (2024), which results in the improved resolution (43 binary digits/metre, compared to previous 10 binary digits/metre) and accuracy of the present study. Nonetheless, the general image and data distribution in the time series remain unchanged. Smoothed curves reflecting ichnotaxa abundance are shown in Figure 2.

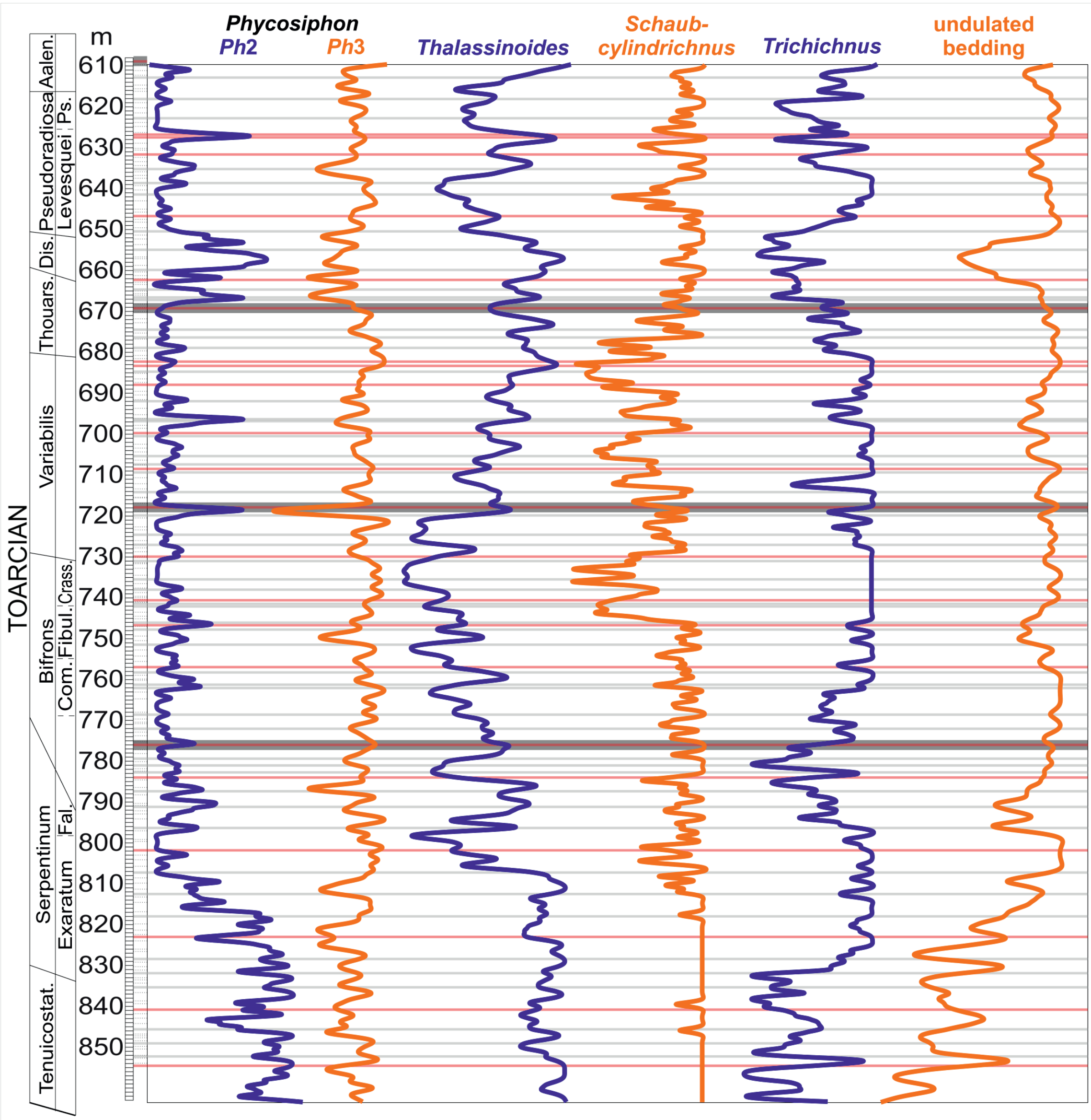

Fig. 2. Spline-smoothed curves for selected ichnotaxa abundance

Toarcian ammonite chronozones and cycle interpretations are from Pieńkowski *et al.* (2024). Thick grey horizontal lines – 1st order cycles (2.4 Myr); red horizontal lines – 2nd order cycles (405 kyr); thin grey horizontal lines – 3rd order cycles (~100 kyr); 4th order cycles not shown

Recurrence is a deterministic property of any dynamical system whose phase space trajectory revisits the same regions of this system's phase space (Marwan *et al.*, 2007). In other words, the recurrence of a state in a time series means that at a certain position, it is arbitrarily similar to another position at another time. In view of this, cyclicity can be regarded as a recurrence with a constant period. Recurrence plots are two-dimensional graphs with axes scaled in the time domain (Fig. 3). Geological data sampled in stratigraphic sections represent the depth domain, which can be treated as equivalent to the time domain, under the assumption that the average sedimentation rate remained constant over the analysed interval. Admittedly, constant sedimentation cannot be assumed for entire c. 9 Myr span of the Toarcian section at Mochras. Still, the location is considered to record relatively stable sedimentation conditions (Pieńkowski *et al.*, 2024), allowing for reliable visualization with recurrence plots.

As a part of recurrence plot rendering, for every pair of times/depths, an evaluation is made of whether or not the two corresponding states are similar. If they are similar, a point is plotted at the corresponding place on the graph (Coco, Dale, 2014). Recurrence plots enable analysis of binary data series because they are generated based on binary matrices. For analysis of continuous data, its binarization with a step function is demanded, which is unnecessary in the case of binary time series (Schmitz, 2000; Hirata *et al.*, 2014). The methodologic nuances of the recurrence plot technique and the principles of their interpretation were explained by Marwan, Kurths (2004) and Marwan *et al.* (2007).

The most basic form of recurrence plot is an auto-recurrence plot based on a single time series (Fig. 4). An extension of this approach exists in the form of cross-recurrence plots, meant to compare the phase space trajectories of two different time series. Cross-recurrence plots allow us to observe simultaneous occurrences of similar states in two different systems. In the present study, an innovative hybrid approach is to combine auto- and cross-recurrence plots, based on raw binary time series and an equivalent smoothed variant of the same series. Original binary time series provide high resolution but also a high amount of observational noise, among manifestations of other stochastic (multifactorial) processes. On the other hand, smoothed data provide a clearer image of deterministic (governed by a few factors) processes, most notably low frequency cyclicities, with the sacrifice of detail. An approach combining both raw and smoothed data was conceived, aiming to achieve a balance between the advantages and disadvantages of both. The outputs shown in Figures 5 and 6 are technically cross-recurrence plots but, because the original time series is compared with its smoothed counterpart, they can be interpreted as if they were auto-recurrence plots. Raw binary time series were smoothed using a smoothing spline algorithm (De Boor, 2001) implemented in PAST software (Hammer *et al.*, 2001) with smoothing factor values in each case experimentally adjusted to obtain an optimal and comparable degree of smoothing.

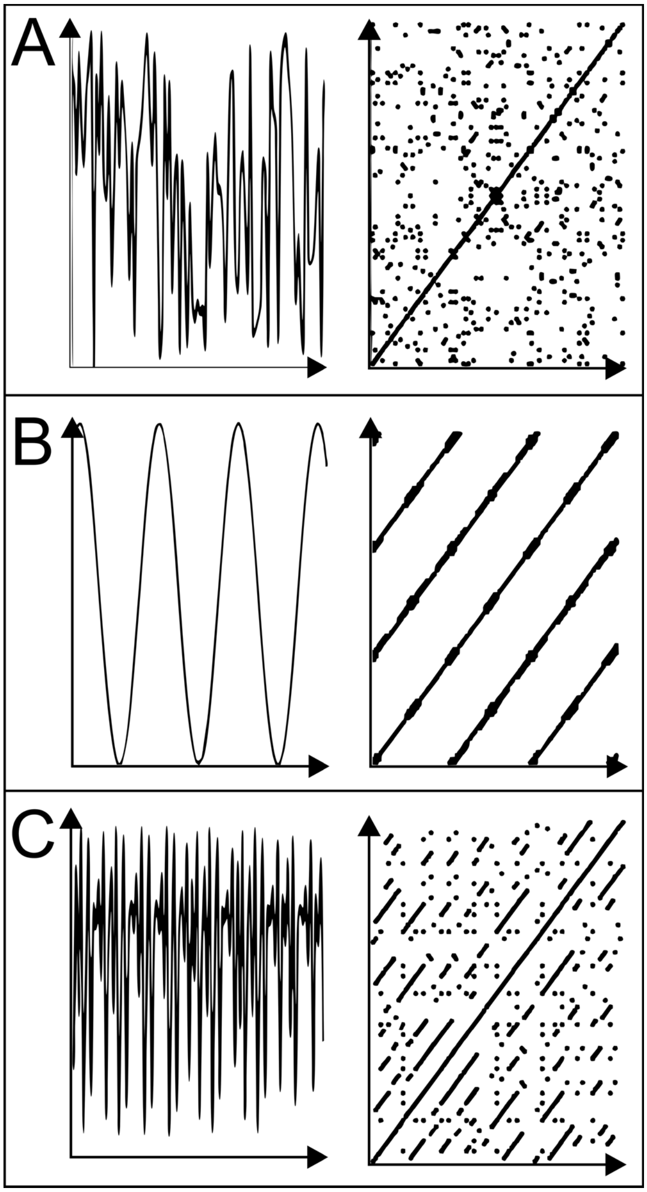

Fig. 3. Example data series (left column) and their recurrence plots (after Coco, Dale, 2014, modified)

A. Stochastic process – noise; **B.** Purely periodic deterministic process – sine wave; **C.** Deterministic chaotic process – logistic map

Estimation of embedding parameters and rendering of recurrence plots was conducted using the Cross Recurrence Plot Toolbox (Marwan *et al.*, 2007) in MATLAB software.

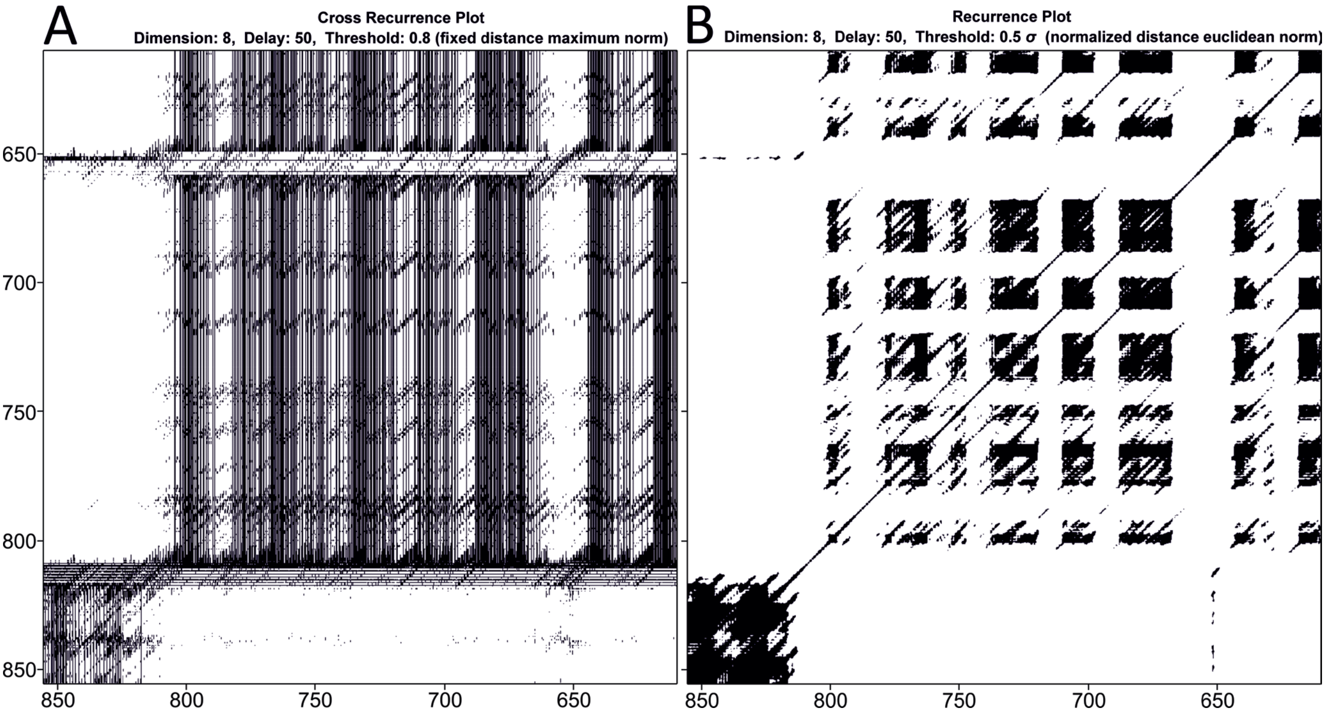

Fig. 4. Auto-recurrence plots of *Phycosiphon* (*Ph*2) occurrences

A. Non-normalised; based on raw (binary) time series; **B.** Normalised to euclidean norm; based on smoothing spline-smoothed time series. Axes scaled in metres below surface

Optimal estimation of three parameters – delay, embedding dimension, and recurrence threshold – is a prerequisite for reliable recurrence plots (Marwan *et al.*, 2007; Hasson *et al.*, 2008; Coco, Dale, 2014). Inadequately low embedding could produce a plot not showing the recurrences that actually occur. Conversely, over-embedding could result in spurious correlations in the plots and artificially abundant long lines (Marwan, 2011). The time-delayed mutual information quantification is a widely used approach for finding the optimal delay. In turn, the false nearest neighbours statistic can serve as guidance for selecting the proper embedding dimension (March *et al.*, 2005). In the present study, the mutual information was computed between the binary and smoothed variants of a particular time series. Delay values read from resultant mutual information graphs were adopted for quantification of the false nearest neighbours graphs. The lowest percentage of false nearest neighbours determined for both binary and smoothed data was very similar for all analysed time series. The obtained delay and embedding dimension parameters (Tab. 1) were used to render recurrence plots. Selection of the optimal threshold value was conducted by trial-and-error, having regard to the principle that the threshold should be as low as possible, but still yield a clear and readable plot (Marwan, 2011; Kraemer *et al.*, 2018). An approach of interdependent neighbours was adopted as a recurrence criterion for cross-recurrence plots.

RESULTS

The results of the present study are in line with those obtained from the same data using spectral analysis (Pieńkowski *et al.*, 2024). In general, all investigated recurrence plots reflect a deterministic chaotic system distinguished by

Table 1

Parameter values used for recurrence plot rendering (see Marwan *et al.*, 2007, for explanation of parameter definition)

	Delay	Embedding dimension	Threshold
Phycosiphon (*Ph*2)	50	8	0.2
Phycosiphon (*Ph*3)	56	5	0.3
Thalassinoides	97	5	0.2
Schaubcylindrichnus	60	5	0.2
Trichichnus	85	7	0.25
undulated bedding	105	5	0.1

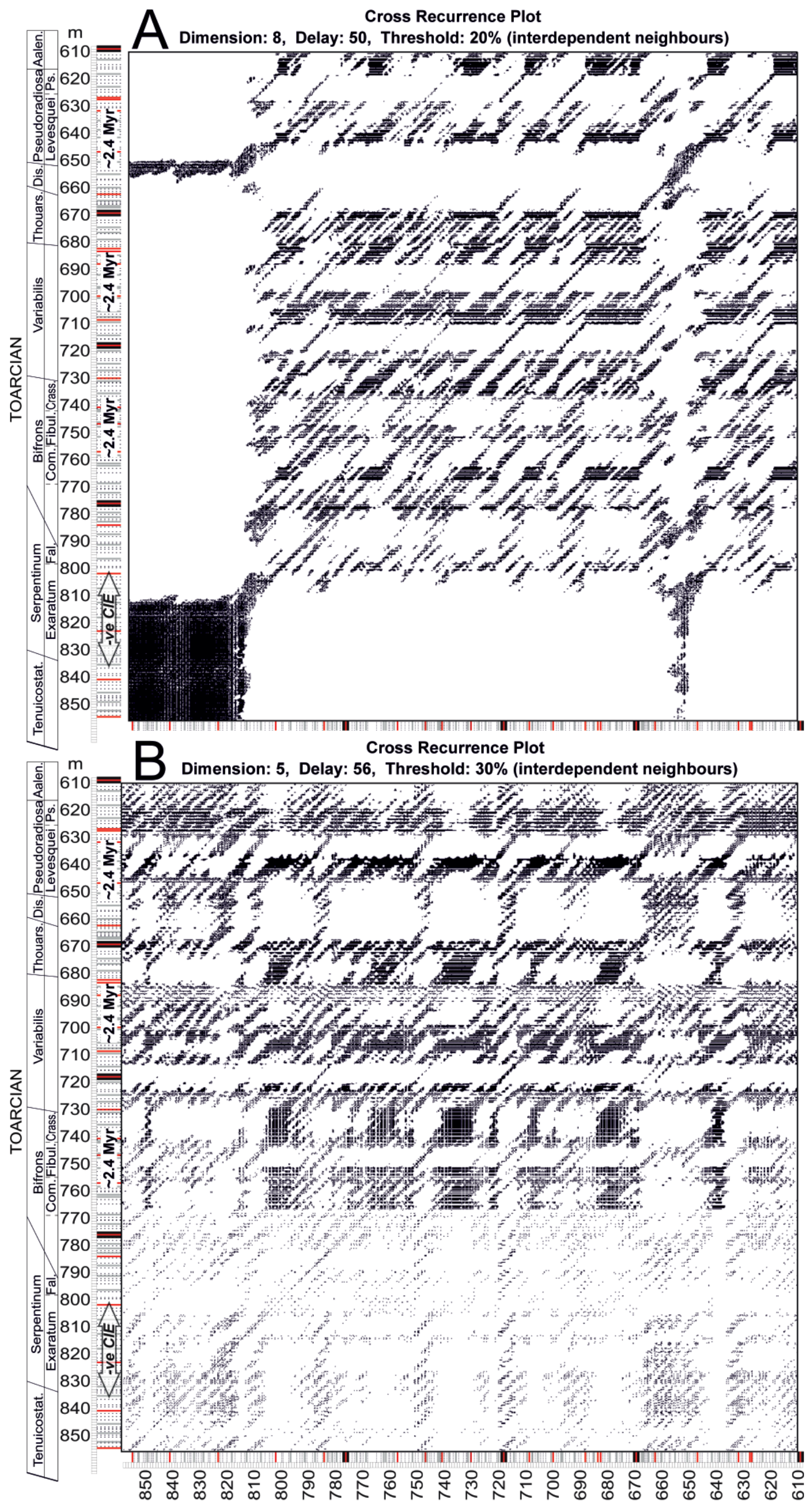

Fig. 5. Cross-recurrence plots of *Phycosiphon* occurrences against the background of Mochras Toarcian zonation and visually determined cyclicity from Pieńkowski *et al.* (2024)

Thin dashed lines – 4th order (c. 20–40 kyr) cycles; solid grey lines – 3rd order (c. 100 kyr) cycles; red lines – 2nd order (c. 405 kyr) cycles; thick black lines – 1st order (c. 2.4 Myr) cycles. **A.** *Phycosiphon* (*Ph*2). **B.** *Phycosiphon* (*Ph*3). Horizontal axes of recurrence plots – binary data, vertical axes – smoothed data

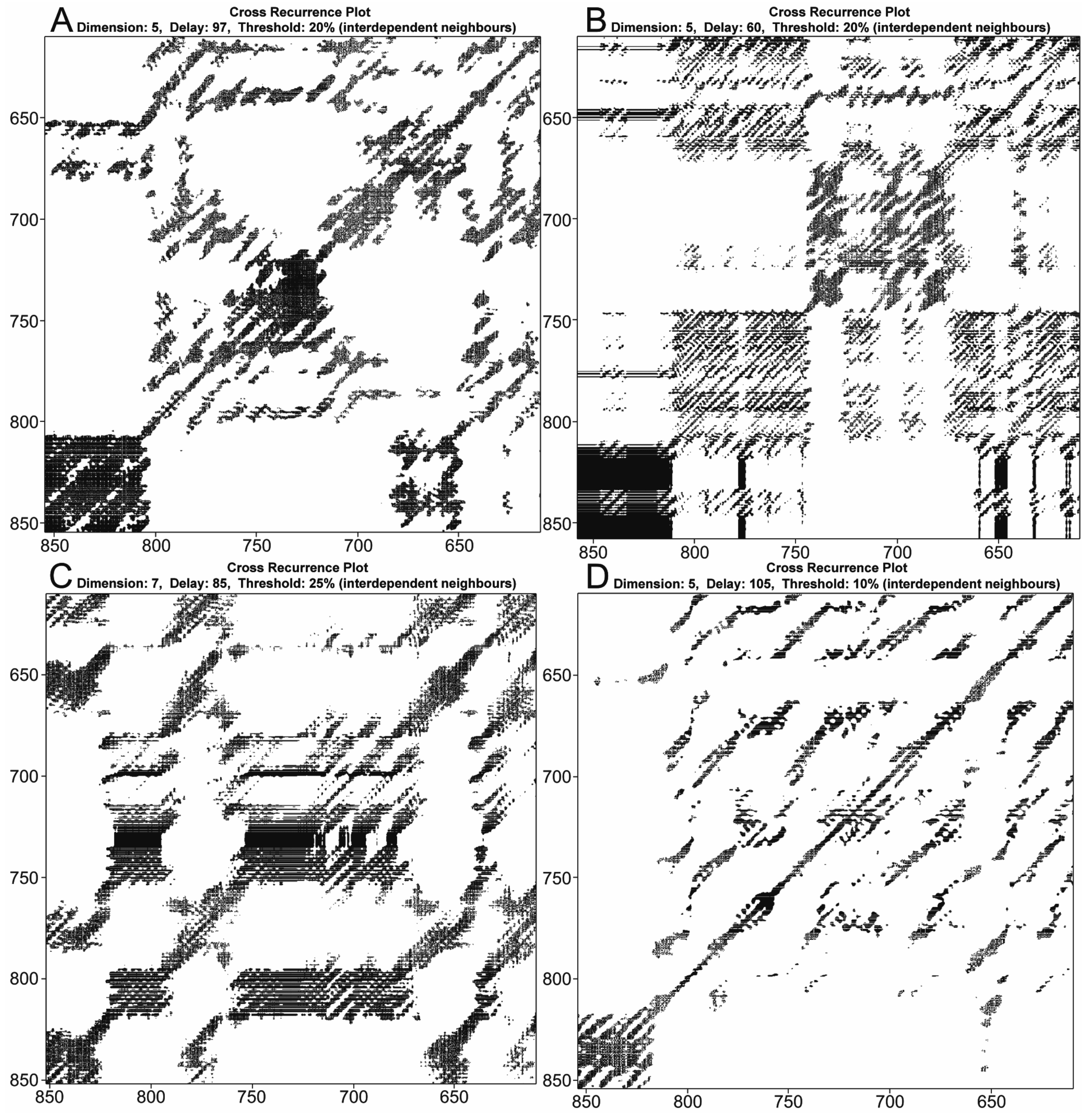

Fig. 6. Cross-recurrence plots based on occurrences of particular ichnotaxa as well as undulated bedding

A. *Thalassinoides*; **B.** *Schaubcylindrichnus*; **C.** *Trichichnus*; **D.** Undulated bedding. Horizontal axes of recurrence plots – binary data, vertical axes – smoothed data

pronounced periodic components (Fig. 3; Marwan, Kurths, 2004; Marwan *et al.*, 2007; Spiridonov, 2017). White areas stem from zeros in the time series, *i.e.*, the absence of a given tracemaker or undulated bedding. Conversely, while black areas are commonly an expression of their occurrence, the pattern displayed by black-shaded areas signifies the nature of the process governing the spatio-temporal distribution of respective trace fossils. Regular patterns, diagonal, vertical, and horizontal lines or alignments of black cells in the recurrence plots reveal the deterministic nature of underlying processes. Vertical and horizontal lines indicate laminarity, meaning that the system persisted and was stable. Regularly spaced diagonal structures, lines, and alignments of black cells signify cyclicity (Marwan *et al.*, 2007; Spiridonov, 2017). Using the example of *Phycosiphon* (*Ph*2) occurrence time series, Figure 4 illustrates the relation between auto-recurrence plots of either raw binary or smoothed time series, and the cross-recurrence plot combining both (Fig. 5A). Hybrid data-based cross-recurrence plots of the remaining time series are shown in Figures 5B and 6.

INTERPRETATION AND DISCUSSION

Particular ichnotaxa and undulated bedding occur asynchronously. The abundance of bioturbation structures produced by opportunistic tracemakers entails a scarcity of highly specialised equilibrium forms and vice versa (Pieńkowski *et al.*, 2021, 2024). The opportunistic tracemakers (the so-called r-selected taxa) quickly colonise substrates under unstable ecological conditions and produce abundant traces but of low diversity, while the equilibrium tracemakers (the so-called K-selected taxa) require favourable and stable ecological conditions, and the abundance of their traces is usually low but diverse (see Ekdale, 1985). Among the discussed trace fossils, *Phycosiphon* represents the opportunistic tracemakers. *Schaubcylindrichnus*, *Trichichnus*, and *Thalassinoides* represent the relatively more equilibrium tracemakers. In the case of *Trichichnus*, the conditions were suitable for its tracemaker but not suitable for others. This is expressed by an increase in abundance of *Trichichnus* at the expense of *Phycosiphon* in some parts of the Toarcian part of the core (Pieńkowski *et al.*, 2024).

Therefore, in the case of high-frequency cycles, recurrent patterns in the plots of respective ichnotaxa are shifted relative to each other. Nonetheless, the intervals between particular diagonal lines remain very similar. Lower-frequency patterns, interpreted as manifestations of 1st and 2nd order cycles, appear in constant positions among the plots.

Recurrence plots of *Phycosiphon* morphotypes *Ph*2 and *Ph*3 show considerable similarity (Fig. 5). Regular patterns of densely distributed diagonal lines can be interpreted as manifestations of the 3rd order cycles. Intervals between these diagonal lines are very similar to those determined by Pieńkowski *et al.* (2024, fig. 2) based on an integrated interpretation of ichnological features. In turn, diagonal dot alignments inside larger-scale lines and structures can possibly reflect the 4th order cyclicity. Apparently, *Phycosiphon Ph*2 and *Ph*3 may also to some extent reflect the 1st order cycles, marked by the thick horizontal lines and edges of the main blocky structures in the plots, which coincide with the limits of the 1st order cycles from Pieńkowski *et al.* (2024; fig. 2).

In the case of *Thalassinoides*, the power spectrum of its occurrences (fig. 9b in Pieńkowski *et al.*, 2024) predominantly displays peaks in the range of precession, apart from a relatively low peak interpreted as short eccentricity. The recurrence plot reflects predominance of precession with densely distributed dot alignments arranged in larger-scale diagonal lines (Fig. 6A). The power spectrum of *Schaubcylindrichnus* (fig. 9b in Pieńkowski *et al.*, 2024) displays peaks in the range of short eccentricity and all shorter component terms of the 4th order cycles. Regularly distributed diagonal lines, presumably reflecting short eccentricity terms occur over most of the recurrence plot (Fig. 6B), with the most striking representation in 740–820 m section. Presumably, long eccentricity (2nd order cycle) may be superimposed over these, as indicated by the fact that some of the diagonal structures are thickened. In turn, the recurrence plot of *Trichichnus* occurrences (Fig. 6C) is composed principally of large-scale diagonal structures as well as regions devoid of well-expressed recurrences at 790–820 and 710–750 m below surface.

Both recurrence plots of *Schaubcylindrichnus* (Fig. 6B) and *Trichichnus* (Fig. 6C) occurrences clearly display transitions between more stochastic and more deterministic dynamics. Furthermore, *Schaubcylindrichnus* occurrences reveal a large-scale checkerboard-like pattern fitting the period lengths of 1st order cycles and reflecting particular susceptibility of respective tracemaker to grand eccentricity-driven (~2.4 Myr) circulation changes (Pieńkowski *et al.*, 2021, 2024). While 610–675 and 750–810 m intervals are characterised by a predominance of higher-frequency 4th and 3rd order cyclicities, the 675–750 m interval is in turn dominated by lower-frequency cycles that can be attributed to 2nd order cyclicities. In the case of *Trichichnus*, the same part of the plot only displays laminar (slowly changing) dynamics.

The recurrence plot of undulated bedding occurrences (Fig. 6D) only to the smallest degree displays structures that could be interpreted as 4th and 3rd order cycles. Dotted and horizontally hatched patterns inside the diagonal structures lack a smaller-scale diagonal orientation and thus probably express stochastic fluctuations in the sedimentary environment. Instead, intervals between diagonal lines/structures in the plot of undulated bedding occurrences are in the range expected for 2nd order cycles. Their length and continuity support such interpretation, as long eccentricity is notable for its stability over very long timespans compared to remaining orbital terms (*e.g.*, Kent *et al.*, 2018). It cannot be excluded that diagonal structures representing 1st order cycles are superimposed on these of 2nd order, exhibiting linear alignments spaced from the main diagonal line by an interval similar to that of 1st order cycles (Fig. 5; fig. 2 in Pieńkowski *et al.*, 2024). It can be hypothesised that undulated bedding, as well as *Thalassinoides* and *Trichichnus*, were predominantly preserved during eccentricity minima. In the opposite were the case, one would expect their occurrences to also reflect precession to a greater degree (see *e.g.*, Hollaar *et al.*, 2023, with respect to other palaeoenvironmental proxy data from the Mochras Pliensbachian). Furthermore, the plot of undulated bedding occurrences displays deflection of diagonal structures at 795–800 m below surface. The cause of this phenomenon remains an open question, but perhaps it can be related to disturbances in activity of benthic organisms coinciding with the end of the Early Toarcian carbon isotope excursion (-ve CIE). Remaining plots that strongly reflect 3rd order cycles in place of isolated 2nd order cyclicity, do not show such deflection, but an interruption of recurrent patterns around c. 800 m can be seen in the cases of both *Phycosiphon* morphotypes and *Thalassinoides.*

The Early Toarcian negative carbon isotope excursion linked with the Toarcian Oceanic Anoxic Event is clearly evident in the reported data (800–835 m; Xu *et al.*, 2018; Ruhl *et al.*, 2022; Pienkowski *et al.*, 2024). In the succession of Mochras, oxygen deficiency occurs earlier than for most other records of this event, during the Tenuicostatum Zone and through the onset of the Serpentinum Zone (870–820 m; Pieńkowski *et al.*, 2024). That dysoxic interval is marked along the left and lower edges of all recurrence plots but is exceptionally distinguished by the stochasticity displayed in the respective intervals of *Phycosiphon* (*Ph*2), *Thalassinoides* and *Schaubcylindrichnus* occurrences. Apart from oxygen deficiency, benthic life development may have been affected by coincident warming of western Tethys bottom water by c. 3°C from the later Tenuicostatum Zone into the early Serpentinum Zone (Ullmann *et al.*, 2020).

CONCLUSIONS

Comparative analysis of ichnological time series using the recurrence plot technique is a promising approach, allowing observation of the cyclic nature of particular ichnotaxa occurrences at different scales simultaneously. A new method of intercomparing raw binary and smoothed time series provides a balance between the high resolution of original data and the clarity of noise-reduced derivative data. The results of the present study are consistent with those obtained previously using spectral analysis, additionally allowing us to observe the changes in dominant cyclic patterns in the spatio-temporal domain. Recurrent patterns of ichnotaxa and undulated bedding from the Mochras core appear to have shifted to some extent due to the mutually exclusive occurrence of their tracemakers. However, the intervals between these patterns remain constant, signifying the pervasiveness and continuity of orbital forcing control over the occurrence of tracemakers. The appearance of recurrence plots implies that occurrence of ichnotaxa was governed by a deterministic chaotic process with well-expressed cyclic components. High frequency cyclicities of the 4th order and, predominantly, the 3rd order are displayed by recurrence plots of both *Phycosiphon* morphotypes and *Schaubcylindrichnus*. Admittedly, tracemakers of these could be influenced by all astronomical cyclicities, but to the greatest extent by the combined effect of precession and obliquity, as well as short eccentricity. In turn, recurrence plots of *Thalassinoides*, *Trichichnus*, and undulated bedding occurrences show less dense patterns of diagonal structures spaced by larger intervals that correspond to those of the 2nd order cycles, indicating that the conditions favourable for the development of undulated bedding, *Thalassinoides*, and *Trichichnus* tracemakers were principally controlled by the long eccentricity.

Acknowledgments. The research is financed by the National Science Centre, Poland, from the programme Opus 13, Grant Agreement No. 2017/25/B/ST10/02235 and the internal Polish Geological Institute Grant No. 62.9012.2016.00.0. This is a contribution to the ICDP and NERC JET Project: SPH was supported from the Natural Environment Research Council (NERC), Grant No. NE/N018508/1. We gratefully acknowledge Polish high-performance computing infrastructure PLGrid (HPC Center: ACK Cyfronet AGH) for providing computer facilities and support within computational grant no. PLG/2024/017118. Norbert Marwan is thanked for providing the CRP Toolbox. Maciej Niezgoda supported the development of BinartGeo.exe program. The reviews by Francisco J. Rodríguez-Tovar (Granada, Spain) and Andrej Spiridonov (Vilnius, Lithuania) and comments by the editor Hubert Wierzbowski helped to improve the manuscript.

Availability of data. Dataset analysed in this study is available in RODBUK Cracow Open Research Data Repository: https://doi.org/10.57903/UJ/GY09BA.

REFERENCES

COCO M.I., DALE R., 2014 – Cross-recurrence quantification analysis of categorical and continuous time series: an R package. *Frontiers in Psychology*, **5**: 510.

COPESTAKE P., JOHNSON B., 2013 – Lower Jurassic Foraminifera from the Llanbedr (Mochras Farm) Borehole, North Wales, UK. *Palaeontonographical Society Monograph*, **641**: 1–403.

DE BOOR C., 2001 – A practical guide to splines. Springer, New York.

DOBSON M.R., WHITTINGTON R.J., 1987 – The geology of Cardigan Bay. *Proceedings of the Geologists' Association*, **98**: 331–353.

EKDALE A.A., 1985 – Paleoecology of the marine endobenthos. *Palaeogeography, Palaeoclimatology, Palaeoecology*, **50**, 1: 63–81.

HAMMER Ø., HARPER D.A., RYAN P.D., 2001 – Past: paleontological statistics software package for education and data analysis. *Palaeontologia Electronica*, **4**, 1: 1–9.

HASSON C.J., van EMMERIK R.E., CALDWELL G.E., HADDAD J.M., GAGNON J.L., HAMILL J., 2008 – Influence of embedding parameters and noise in center of pressure recurrence quantification analysis. *Gait & Posture*, **27**, 3: 416–422.

HESSELBO S.P., BJERRUM C.J., HINNOV L.A., MACNIOCAILL C., MILLER K.G., RIDING J.B., van de SCHOOTBRUGGE B., the Mochras Revisited Science Team, 2013 – Mochras borehole revisited: A new global standard for Early Jurassic Earth history. *Scientific Drilling*, **16**: 81–91.

HINNOV L.A., 2000 – New perspectives on orbitally forced stratigraphy. *Annual Review of Earth and Planetary Sciences*, **28**, 1: 419–475.

HIRATA Y., LANG E. J., AIHARA K., 2014 – Recurrence plots and the analysis of multiple spike trains. *In:* Springer Handbook of Bio-/Neuroinformatics (Ed. N. Kasabov): 735–744. Springer, Berlin – Heidelberg.

HOLLAAR T.P., HESSELBO S.P., DECONINCK J.F., DAMASCHKE M., ULLMANN C.V., JIANG M., BELCHER C.M., 2023 – Environmental changes during the onset of the Late Pliensbachian Event (Early Jurassic) in the Mochras Borehole, Cardigan Bay Basin, NW Wales. *Climate of the Past*, **19**: 979–997.

KENT D.V., OLSEN P.E., RASMUSSEN C., LEPRE C., MUNDIL R., IRMIS R. B., GEHRELS G.E., GIESLER D., GEISSMAN J.W., PARKER W.G., 2018 – Empirical evidence for stability of the 405-kiloyear Jupiter – Venus eccentricity cycle over hundreds of millions of years. *Proceedings of the National Academy of Sciences*, **115**, 24: 6153–6158.

KRAEMER K.H., DONNER R.V., HEITZIG J., MARWAN N., 2018 – Recurrence threshold selection for obtaining robust recurrence characteristics in different embedding dimensions. *Chaos*, **28**, 8: 085720.

MARCH T.K., CHAPMAN S.C., DENDY R.O., 2005 – Recurrence plot statistics and the effect of embedding. *Physica D: Nonlinear Phenomena*, **200**, 1/2: 171–184.

MARWAN N., 2011 – How to avoid potential pitfalls in recurrence plot based data analysis. *International Journal of Bifurcation and Chaos*, **21**, 4: 1003–1017.

MARWAN N., KURTHS J., 2004 – Cross recurrence plots and their applications. *In*: Mathematical Physics Research at the Cutting Edge (Ed. C.V Benton): 101–139. Nova Science, Hauppauge.

MARWAN N., ROMANO M.C., THIEL M., KURTHS J., 2007 – Recurrence plots for the analysis of complex systems. *Physics Reports*, **438**, 5/6: 237–329.

MARWAN N., DONGES J.F., DONNER R.V., EROGLU D., 2021 – Nonlinear time series analysis of palaeoclimate proxy records. *Quaternary Science Reviews*, **274**: 107245.

PIEŃKOWSKI G., UCHMAN A., NINARD K., HESSELBO S.P., 2021 – Ichnology, sedimentology, and orbital cycles in the hemipelagic Early Jurassic Laurasian Seaway (Pliensbachian, Cardigan Bay Basin, UK). *Global and Planetary Change*, **207**: 103648.

PIEŃKOWSKI G., UCHMAN A., NINARD K., PAGE K.N., HESSELBO S.P., 2024 – Early Jurassic extrinsic solar system dynamics versus intrinsic Earth processes: Toarcian sedimentation and benthic life in deep-sea contourite drift facies, Cardigan Bay Basin, UK. *Progress in Earth and Planetary Science*, **11**, 1: 18.

RUHL M., HESSELBO S.P., JENKYNS H.C., XU W., SILVA R.L., MATTHEWS K.J., MATHER T.A., MAC NIOCAILL C., RIDING J.B., 2022 – Reduced plate movement controlled onset and timing of Early Jurassic (Toarcian) Karoo-Ferrar large igneous province volcanism and global environmental change. *Science Advances*, **8**: eabo0866

SCHMITZ A., 2000 – Measuring statistical dependence and coupling of subsystems. *Physical Review E*, **62**, 5: 7508.

SPIRIDONOV A., 2017 – Recurrence and cross recurrence plots reveal the onset of the Mulde event (Silurian) in the abundance data for Baltic conodonts. *The Journal of Geology*, **125**, 3: 381–398.

SPIRIDONOV A., BALAKAUSKAS L., STANKEVIČ R., KLUCZYNSKA G., GEDMINIENĖ L., STANČIKAITĖ M., 2019 – Holocene vegetation patterns in southern Lithuania indicate astronomical forcing on the millennial and centennial time scales. *Scientific Reports*, **9**, 1: 14711.

SPIRIDONOV A., SAMSONĖ J., BRAZAUSKAS A., STANKEVIČ R., MEIDLA T., AINSAAR L., RADZEVIČIUS S., 2020 – Quantifying the community turnover of the uppermost Wenlock and Ludlow (Silurian) conodonts in the Baltic Basin. *Palaeogeography, Palaeoclimatology, Palaeoecology*, **549**: 109128.

ULLMANN C.V., BOYLE R., DUARTE L.V., HESSELBO S.P., KASEMANN S.A., KLEIN T., LENTON T.M., PIAZZA V., ABERHAN M., 2020. – Warm afterglow from the Toarcian Oceanic Anoxic Event drives the success of deep-adapted brachiopods. *Scientific Reports*, **10**: 6549.

WALTHAM D., 2015 – Milankovitch period uncertainties and their impact on cyclostratigraphy. *Journal of Sedimentary Research*, **85**, 8: 990–998.

WESTERHOLD T., MARWAN N., DRURY A.J., LIEBRAND D., AGNINI C., ANAGNOSTOU E., BARNET J.S.K., BOHATY S.M., de VLEESCHOUWER D., FLORINDO F., FREDERICHS T., HODELL D.A., HOLBOURN A.E., KROON D., LAURETANO V., LITTLER K., LOURENS L.J., LYLE M., PÄLIKE H., RÖHL U., TIAN J., WILKENS R.H., WILSON P.A., ZACHOS J.C., 2020 – An astronomically dated record of Earth's climate and its predictability over the last 66 million years. *Science*, **369**: 1383–1387.

WOODLAND A. (Ed.), 1971 – The Llanbedr (Mochras Farm) Borehole. *Institute of Geological Sciences, Report* **71**, 18: 1–116.

XU W., RUHL M., JENKYNS H.C., LENG M.J., HUGGETT J.M., MINISINI J.M., ULLMANN C.V., RIDING J.B., WEIJERS J.W.H., STORM M.S., HESSELBO S.P., 2018 – Evolution of the Toarcian (Early Jurassic) carbon-cycle and global climatic controls on local sedimentary processes (Cardigan Bay Basin, UK), *Earth and Planetary Science Letters*, **484**: 396–411.

SOFTWARE:

N. MARWAN: Cross Recurrence Plot Toolbox for MATLAB®, Ver. v5.29 (R38).

M. NIEZGODA: BinartGeo.exe, raster binarization program.